STAR, A Sprawl Tuned Autonomous Robot

David Zarrouk[1], Andrew Pullin[2], Nick Kohut[2], Ronald S. Fearing[1]

Abstract— **This paper presents a six-legged, sprawl-tuned autonomous robot (STAR). This novel robot has a variable leg sprawl angle in the transverse plane to adapt its stiffness, height, and leg-to-surface contact angle. The sprawl angle can be varied from nearly positive 60 degrees to negative 90 degrees, enabling the robot to run in a planar configuration, upright, or inverted (see movie). STAR is fitted with spoke wheel-like legs which provide high electromechanical conversion efficiency and enable the robot to achieve legged performance over rough surfaces and obstacles, using a high sprawl angle, and nearly wheel-like performance over smooth surfaces for small sprawl angles. Our model and experiments show that the contact angle and normal contact forces are substantially reduced when the sprawl angle is low, and the velocity increases over smooth surfaces, with stable running at all velocities up to 5.2m/s and a Froude number of 9.8.**

I. INTRODUCTION

Drawing inspiration from insects, miniature crawling robots possess substantial advantages over wheeled vehicles for off-road locomotion, such as in caves and collapsed buildings, for reconnaissance and search and rescue purposes. Their low weight and cost allow their deployment in large numbers, independently or in swarms, to cover a large work area and increase the odds that some of the robots will succeed in performing a specific task. Some existing examples of comparable robots can crawl at more than 5 (and up to 15) body lengths per second, such as Mini-Whegs [10], Dyna-RoACH [4], DASH [1], iSprawl [6], OctoRoACH [11], RHex [3], and Sprawlita [2]. Since it is difficult to implement active leg joints at this scale, a key challenge in developing a high speed and highly maneuverable miniature crawler is the design of passive mechanical elements which contribute to the stability of the robot during locomotion, similar to insects [8][5]. The crawling mechanism can be approximated using the spring loaded inverted pendulum model (SLIP) [14][15], which describes the locomotion of insects in the sagittal plane.

In-plane or lateral models of locomotion which neglect vertical oscillation, but are useful for steering and yaw stability, were investigated by Schmitt and Holmes [12] [13], Kukillaya and Holmes [9], and Seipel et al [16] who studied the dynamic locomotion model of cockroaches. The lateral leg spring model (LLS) shows that sprawled angle postures are stable both in the sagittal lateral plane at different speeds, and that the sprawled posture is more energy efficient. Full et al. presented a first sprawled robot, SprawlHex [7], which can adjust its sprawl angle, up to 20 degrees, in order to experimentally compare to animal behavior.

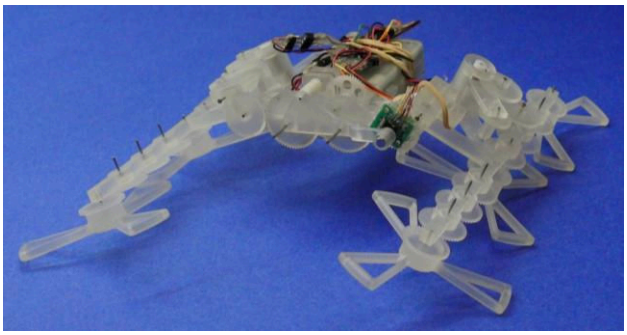

Figure 1. The sprawl-tuned autonomous robot has three motors, one for each side of the legs and a third motor which actuates the sprawl angle.

The sprawl-tuned autonomous robot (or STAR), presented in this work, is an autonomous crawler that has a variable sprawl angle to adapt its legs to different surfaces. Inspired by SprawlHex and Mini-Whegs, this design allows the robot to transform its locomotion mechanics from the sagittal plane to the lateral plane and combines the advantages of both vertical and in-plane locomotion. At low sprawl angles, the vertical contact angle of the foot with the surface is reduced which minimizes collisions and reduces the uncontrolled vertical dynamics, resulting in smooth operation of the robot at all speeds. The sprawl angle can also be used to change the width and height of the robot in order to fit between, above, or underneath obstacles. The characteristic length of the robot is 12 cm and the weight is 73 grams including battery and control board for autonomous operation. To improve stability and energy consumption, the robot is fitted with radially spoked legs which can perform almost like regular wheels for low sprawl angles and as legs for high sprawl angles.

In this paper, we first present the mechanical design of the robot in Section II. In section III we present the analysis and design considerations of the robot and the effect of the sprawl angle on locomotion. In Section IV we present the experimental results of the robot being run over different surface conditions.

II. MEHANICAL DESIGN

The primary design goal of STAR is to achieve a small, low cost, fast, highly-maneuverable and stable platform

[1] Department of EECS, UC Berkeley, (zadavid@berkeley.edu).
[2] Department of ME, UC Berkeley.

which is adaptable to different surface conditions. These goals can be achieved by minimizing the collision of the legs with the ground through variable leg geometry and compliance, thus reducing the uncontrolled vertical dynamics.

A. Robot and leg design

STAR has a rigid body core which holds the onboard battery and the control board. Each side of the robot has three-spoke legs with drive distributed from a single motor to all three legs. A constant mechanical 60° rotational phase offset between neighboring legs reduces the aerial phase and collision with the ground of the robot. Each of the three legs and their motor are fixed on the same rigid link which is attached to the robot through a rotational pin joint. The relative angle between the legs and the main body, as presented in Figure 2, forms the sprawl angle, which is defined as ρ=0 when the legs are coplanar with the ground. The positive sense of the sprawl angle is as shown. The sprawl angles at both sides are actuated symmetrically through a single motor and mechanism to insure identical sprawl on both sides.

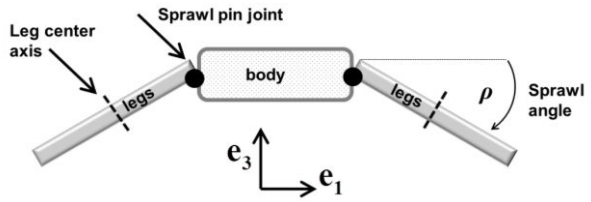

Figure 2. Front view of sprawl robot.

The sprawl angle can be varied in the range (+60°, -90°), as shown in Figure 3, allowing the robot to continue running in the same direction even when upside down.

The spoke wheel legs are composed of three compliant legs attached to a main hub (see Figure 4). The length of each spoke L_{leg} is 28 mm, and the tip of the leg has a circular shape spanning α_{solid}=30°. The gap angle, α_{gap}, between the edges of the leg spokes is 90°, which allows the tips of the legs to reach up to 4cm high for crawling over obstacles.

C. Actuation and control

Each set of legs is driven by a 7 mm brushed DC motor (Didel MK07-3.3), and a transmission with a ratio of 48:1. For high speed we used a 16:1 ratio and (Didel MK07-2.3) motors. The high ratio ensures high torque output and steady velocity. The robot uses a 300mA-hr LiPo, 4V battery from Full River giving 30 minutes endurance when running at full drive capacity.

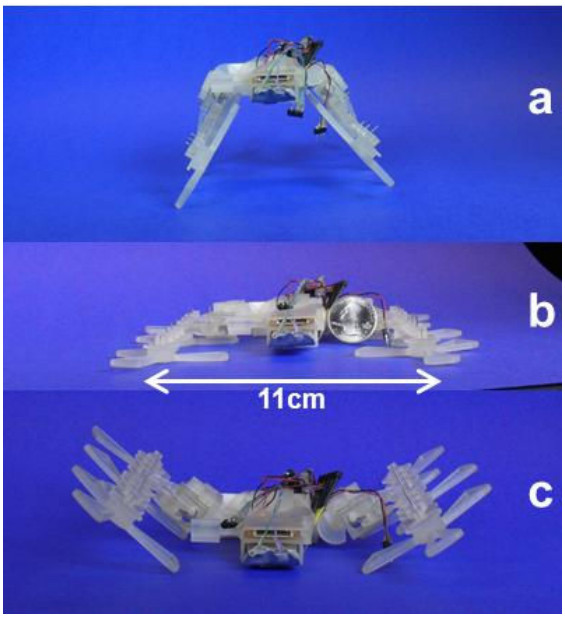

Figure 3. STAR at different sprawl angles. a) Positive sprawl angle. b) Zero sprawl angle. c) Negative sprawl angle.

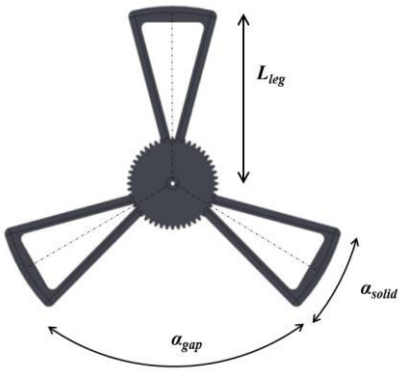

Figure 4. Spoke leg wheels.

Similar to OctoRoACH [11], the leg set on each of the two sides are not phase synchronized, and STAR uses differential velocity for steering using a closed loop controller, where the yaw rate of the robot is measured using the onboard MEMS gyro and the velocity of the motor is measured from the motor back EMF.

D. Manufacturing

STAR is designed for rapid manufacturing; the body core, motor housing, spur gears, and legs are 3D printed using a Projet 3000 machine. The printer's accuracy is roughly 0.05mm. The robot is designed for easy assembly and simple part replacement, and the total mechanical assembly requires roughly 30 minutes.

III. ANALYSIS AND DESIGN CONSIDERATIONS

In this section, we analyze the effect of the sprawl angle on the sagittal velocity during running, the leg-to-surface contact angle, and the normal compliance of the robot.

A. Sagittal velocity and leg-to-surface contact angle

1) *90 degree sprawl angle*

The analysis of the contact angle β of the legs to the ground allows us to estimate the contact normal, sagittal, and thrust forces acting on the robot, which dictate the running performance and stability. We first look at the contact angle of the legs when the sprawl angle is 90 degrees and the robot is quasistatic (Figure 5). In this case, the contact angle at zero speed, β_0, will be in the sagittal plane and its value will vary depending on the stability of the robot

$$\frac{\alpha_{gap}}{4} \le \beta_0 \le \frac{\alpha_{gap}}{2} \tag{1}$$

The variation of the stance height of the robot during a cycle while in contact with the ground is

$$\Delta h = L_{leg}\left(1-\cos\left(\beta_0\right)\right) \tag{2}$$

The lower limiting value of β_0 has two main advantages. First it reduces normal impact forces to the ground. Second, it reduces the change in height through a stride and thereby decreases the power requirements of the motor and improves stability. Adding more legs to the spoke wheels will further reduce the contact angle but the performance becomes similar to wheels. As the robot runs faster, the contact angle will increase which results in higher normal forces.

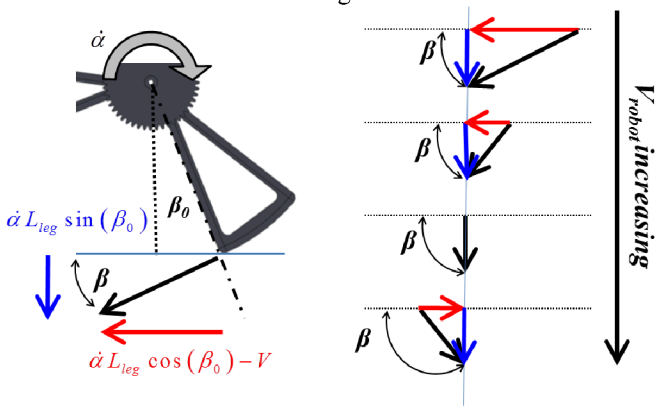

Figure 5. The contact angle β of the leg with the ground for 90° sprawl angle as function of robot speed.

2) General sprawl angle

When the axis of rotation is sprawled by an angle ρ, the change in height of the robot through a stride is

$$\Delta h = L_{leg}\left(1-\cos\left(\beta_0\right)\right)\sin\left(\rho\right) \tag{3}$$

the velocity of the legs as function of the sprawl angle is constant

$$V_{leg/robot} = \dot{\alpha} L_{leg} \tag{4}$$

However, the velocity of the legs relative to the ground is a function of the velocity of the robot.

$$\mathbf{V_{leg}} = \mathbf{V_{robot}} + \mathbf{V_{leg/robot}} \tag{5}$$

Neglecting the velocities in the $\mathbf{e_1}$ and $\mathbf{e_3}$ direction, the velocity of the contact point of the leg relative to surface

$$\mathbf{V_{leg}} = \begin{pmatrix} \cos\left(\rho\right)\sin\left(\beta_0\right)\dot{\alpha} L_{leg} \\ V_{robot} - \cos\left(\beta_0\right)\dot{\alpha} L_{leg} \\ -\sin\left(\rho\right)\sin\left(\beta_0\right)\dot{\alpha} L_{leg} \end{pmatrix} \tag{6}$$

and the contact angle of the leg to the surface is

$$\beta = a\tan\frac{\dot{\alpha} L_{leg}\sin\left(\rho\right)\sin\left(\beta_0\right)}{\left\{\left(V_{robot} - \dot{\alpha} L_{leg}\cos\left(\beta_0\right)\right)^2 + \left(\dot{\alpha} L_{leg}\cos\left(\rho\right)\sin\left(\beta_0\right)\right)^2\right\}^{0.5}} \tag{7}$$

Where, in our case, the angle β_0 as per Eq. (1) ranges between 22.5° and 45°. Figure 6 presents the contact angle β as a function of the sprawl angle and advance ratio. Beyond an advance ratio of $1/\sqrt{2}$, the contact angle becomes negative and, as a result, the first impact to the surface is causing negative thrust.

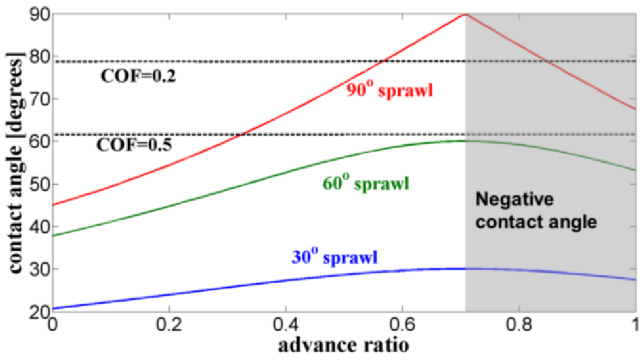

Figure 6. The interval of the contact angle as function of the sprawl angle and advance ratio.

It is noted that beyond the friction angle, the legs cannot slide which may increase the traction but may also result in significant collision with the ground if the locomotion is not smooth.

C. Vertical compliance

The normal compliance of the robot is mainly due to the bending of the legs and torsional compliance of the gears. The legs can be approximated as a simple beam with inertia

moment I_{leg}. The vertical compliance is the combination in series of the bending, torsion, and shortening of the leg. If we assume that the legs are rigid along their length, the total normal compliance of the legs as a function of the sprawl angle is

$$k_n = \frac{1}{L_{leg}^2 \cos(\rho)} \left(k_r + 3\frac{EI}{L_{leg}} \right)^{-1} \quad (8)$$

which, in this case, shows that the normal compliance is a decreasing function of the sprawl angle only. Figure 8 presents the variation of the normal stiffness, divided by the stiffness at zero sprawl , as a function of the sprawl angle. At 75 degrees, the relative stiffness increases by four fold.

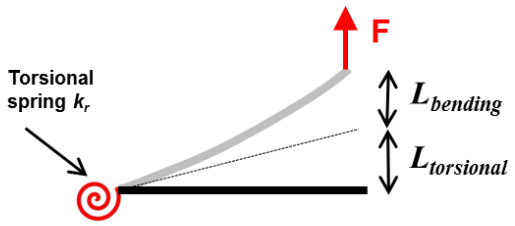

Figure 7. Showing the normal compliance due to bending and torsional compliance.

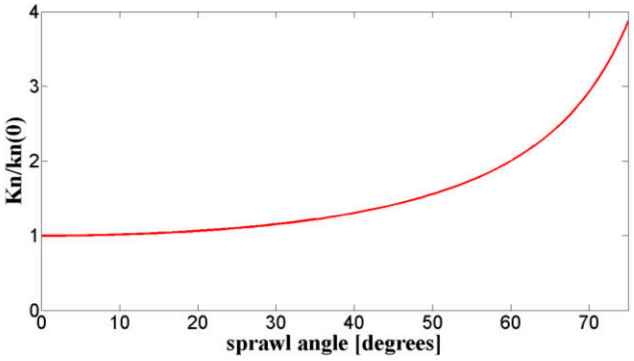

Figure 8. Normal stiffness k_n, divided by the stiffness at $k_n(0)$ at ρ=0, as a function of the sprawl angle.

E. Switching the locomotion direction

When the robot is configured to a slight negative sprawl angle (ρ=0), the thrust of the legs will reverse due to the legs making contact to the ground on the inside of the swing rather on the outside. With onboard actuated sprawl angle, this mechanism could be used to spontaneously reverse direction or reverse thrust braking without changing the spin direction of the legs.

IV. RESULTS

In this section we present the experimental results of our robot, with various sprawl angles, running over different surface conditions, and performing various maneuvers.

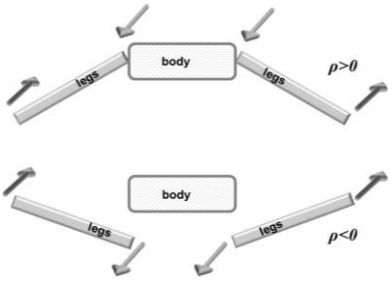

Figure 9. Robot front view. Slightly negative sprawl angle causes the robot to run in the opposite direction without changing the rotation direction of the legs.

A. Velocity and stability

In order to investigate the locomotion performance of the robot as a function of its sprawl angle, we ran the robot over horizontal plywood and carpet surfaces and over a 10 degree incline. The input velocity profile was composed of acceleration (one second), constant velocity (three seconds) and deceleration (one second). The robot's nominal velocity (as if equipped with regular wheels) during the constant speed phase was roughly 0.6m/s. Figure 10 shows the average velocity of robot, extracted from the steady state stage, for different sprawl angles. Over horizontal wood surface and with a 15° sprawl angle, the performance is almost identical to that of wheels, but the velocity drops as a function of the sprawl angle. The velocity for upright legs (ρ=90°) was roughly one third smaller, which is similar to what was reported by Morrey et al [10]. When running on an incline, a substantial reduction of speed is observed at a sprawl angle of 45° and beyond, implying that the thrust force is substantially reduced due to increased collisions with the ground.

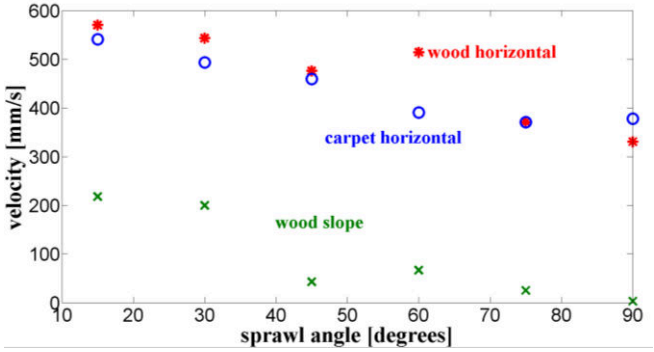

Figure 10. Velocity of the robot as a function of the sprawl angle over three different surfaces.

Figure 11 presents a top view of the trajectory of the robot using closed-loop gyro steering control [11] over carpet as obtained from the Vicon system. For small sprawl angles, the robot is easily capable of traveling straight with practically no error. As the sprawl angle increases, the deviation from straight becomes more significant due to increasing ground contact forces causing disturbances to lateral motion. The maximum heading deviation error for 75° and 90° sprawl angles is respectively 5 and 3.5 degrees.

B. Contact ground forces

In order to investigate the ground reaction forces we use a 3D force plate sensor with a resolution of 0.01 N. The robot was run at roughly 0.5m/s and the sprawl angle was varied from 15 to 90 degrees. Figure 12 presents the average of the instantaneous peak normal forces due to the contact of the legs with the ground. Comparing the two extreme configurations, the normal force is measured to be five times larger at a sprawl angle of 90° than 15°.

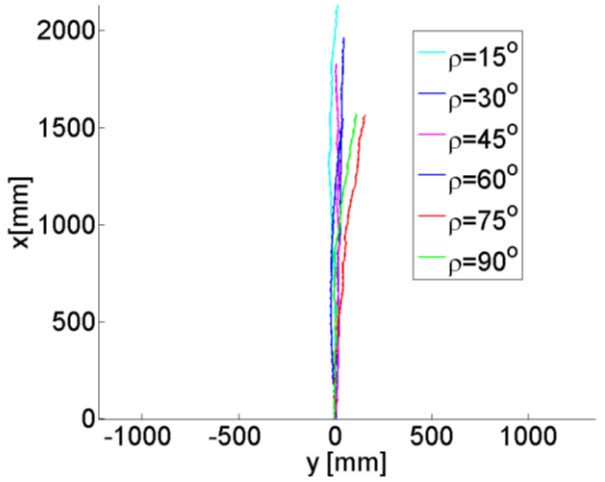

Figure 11. Path of the robot running over horizontal wood surface at different sprawl angles.

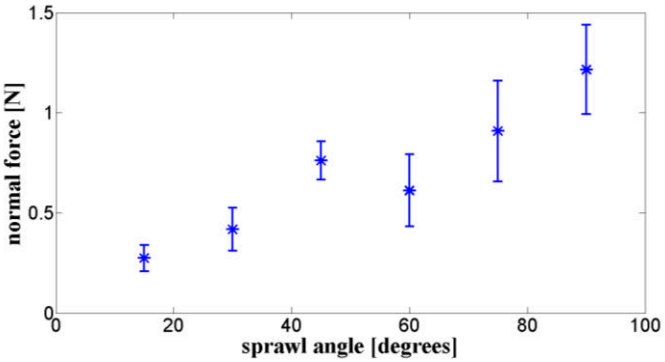

Figure 12. The average normal impact force and standard deviation as function of the sprawl angle.

C. Robot Performance Maneuvers

In this section we present various novel maneuvers that were performed with the robot.

1) Crawling over and under objects

The minimum height of STAR, which is achieved at a sprawl angle of zero degrees, is 25mm. At this angle, the robot cannot advance. Increasing the sprawl to a few degrees, the robot remains practically flat due to its compliance but the ground contact on the external swing of the legs is favored and the robot can advance. This allows the robot to crawl under gaps of approximately 25°. When the legs are upright (ρ=90°), the robot can easily surmount obstacles larger than the spoke length, up to 35mm. Figure 13a and b show the robot crawling both under and over a 30 mm high bridge (whose thickness is 5 mm).

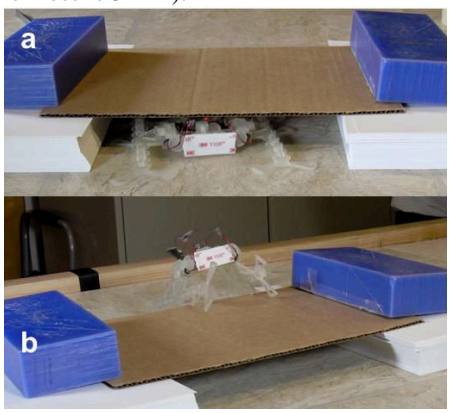

Figure 13. a) The robot is seen crawling underneath the bridge. b) The robot crawling over the top of the same bridge.

2) High speed running and turning performance

During all of our experiments, we used a transmission gear ratio of 48:1. STAR is designed to easily switch to ratios of 24:1 and 16:1 for higher maximum speeds. At low sprawl angle, the locomotion was highly stable and the robot attained 5.2 m/s in straight locomotion, with a deviation from straight of less than one degree. The robot can achieve a 360 degree rotation in less than one second by driving one side at maximum speed and the other at zero. This puts the rotation center at the middle leg of the static side, and the turning radius is roughly 9 cm.

3) Running over stones and obstacles

The robot successfully climbed over a rock bed including obstacles. The robot was able to successfully surmount a rocky incline, traversing a hill with a 30° slope while maintaining its orientation using the steering control.

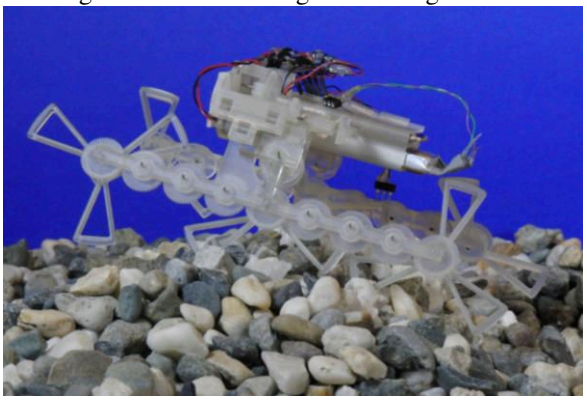

Figure 14. The robot over a rock bed.

4) Negative sprawl angle and inverted running

As previously mentioned, STAR reverses its motion direction when the sprawl angle becomes negative (Figure 15

a). In this configuration, inverting the body will bring the outside swing of the legs in contact with the ground resulting in original direction drive. With this double inversion, all control laws are consistent and leg drive and steering control continue to function as expected.

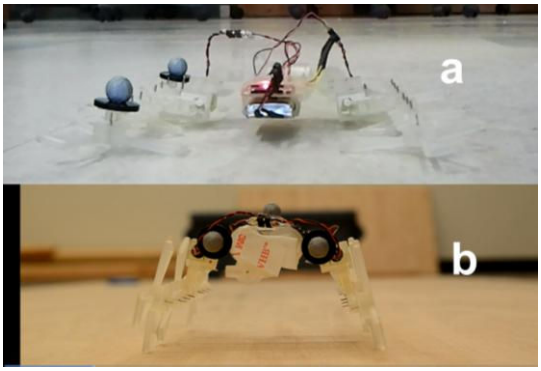

Figure 15. a) STAR with small negative sprawl angle. b) STAR with negative sprawl angle and inverted.

V. CONCLUSIONS

In this paper we present a novel, 12 cm long, sprawl tuned autonomous robot. The sprawl angle of the robot can be reconfigured through almost 150^{o}, which allows it to transform its locomotion dynamics from the sagittal to the horizontal plane and achieve the benefits of both legged and wheeled locomotion. Our analysis shows that the sprawl angle is effective in reducing the contact angle of the leg with the surface even at high velocity, reduces the vertical oscillation of the center of mass, and increases the vertical compliance of the robot to adapt for different surface conditions.

We ran the robot on different flat surface conditions and found that over horizontal surfaces, the robot travels roughly 50% faster, both over wood and carpet, using a low sprawl angle compared to a high sprawl angle. On inclines, the difference was much larger, implying that the robot is losing much of its thrust at high sprawl angles. Furthermore, our experiments show that increasing the sprawl angle from 15 degrees to 90 degrees increased normal ground forces by five fold. Large normal forces are important on challenging surfaces characterized by compliance and low friction, but decrease stability on rigid smooth surfaces. For low sprawl angles, the robot's performance was similar to a comparable wheeled configuration in terms of stability and velocity as the normal forces are small and the center of mass is near the ground.

Through the use of a reconfigurable sprawl angle, this miniature robot presents many unique capabilities and performance moving on varying terrain surfaces and for traversing obstacles.

VI. REFERENCES

[1] P. Birkmeyer, K. Peterson, and R.S. Fearing, "DASH: A dynamic 16g hexapedal robot", IEEE Int. Conf. on Intelligent Robots and Systems, pp. 2683-2689, 2009.

[2] J.G Cham, S.A. Bailey, J.E. Clark, R.J. Full, and M.R. Cutkosky, "Fast and robust: Hexapedal robots via shape deposition manufacturing", *The International Journal of Robotics Research*, Vol. 21, No. 10-11, pp. 869-882, 2002.

[3] K. C. Galloway, G. C. Haynes, B. D. Ilhan, A. M. Johnson. R. Knopf, G. Lynch, B. Plotnick, M. White, D. E. Koditschek, "X-RHex: a highly mobile hexapedal robot for sensorimotor tasks", University of Pennsylvania Technical Report, 2010.

[4] A. M. Hoover, S. Burden, X.Y. Fu, S. S. Sastry, and R. Fearing, "Bio-inspired design and dynamic maneuverability of a minimally actuated six-legged robot", IEEE International Conference on Biomedical Robotics and Biomechatronics, pp. 869-873, 2010.

[5] D. I. Jindrich, and R. J. Full, "Dynamic stabilization of rapid hexapedal locomotion", *Journal of Experimental Biology*, Vol. 205, pp. 2803-2823, 2002.

[6] S. Kim, J. E. Clark, and M. R. Cutkosky, "iSprawl: Design and turning of high-speed autonomous open-loop running", *The Int. Journal of Robotic Research*, Vol. 25, No.9. pp. 903-912, 2006.

[7] H. Komsuoglu, K. Sohn, R. J. Full, D. E. Koditschek, "A physical model for dynamical arthropod running on level ground", 11th ISER, 2008.

[8] T. M. Kubow, and R. J. Full, "The role of the mechanical system in control: A hypothesis of self stabilization in hexapedal runners", *Philosophical Transactions: Biological sciences*, Vol. 354, pp. 849-861, 1999.

[9] R. P. Kukillaya, P. Holmes, "A hexapedal jointed-leg model for insect locomotion in the horizontal plane", *Biol. Cyber.*, DOI 10.1007/s00422-007-0180-2, 2007.

[10] J. M. Morrey, B. Lambrecht, A.D. Horchler, R. E. Ritzmann, and R.D. Quinn, "Highly mobile and robust small quadruped robots", IEEE Int. Conf. on Intelligent Robots and Systems, Vol. 1, pp. 82-87, 2003.

[11] A.O. Pullin, N. J. Kohut, D. Zarrouk, and R.S. Fearing, "Dynamic Turning of 13cm robot comparing tail and differential drive", IEEE Int. Conf. on Robotics and Automation, pp. 5083-5093, 2012.

[12] J. Schmitt, P. Holmes, "Mechanical models for insect locomotion: dynamics and stability in the horizontal plane I. Theory", *Biol. Cyber.* Vol. 83, pp. 501-515, 2000.

[13] J. Schmitt, P. Holmes, "Mechanical models for insect locomotion: dynamics and stability in the horizontal plane II. Application", *Biol. Cyber.* Vol. 83, pp. 517-527, 2000.

[14] J. E. Seipel, P. Holmes, "Running in three dimensions: analysis of a point-mass sprung-leg model". *The International Journal of Robotics Research*, Vol. 24, No. 8, pp. 677-674, 2005.

[15] J. Seipel, and P. Holmes, "A simple model for clock-actuated legged locomotion", *Regular and Chaotic Dynamics*, Vol. 12. No. 5. pp. 502-520, 2007.

[16] J. E. Seipel, P. J. Holmes, and R. J. Full, "Dynamics and stability of insect locomotion: a hexapedal model for horizontal plane motions", *Biol. Cyber.* Vol. 91, pp. 6-90, 2004.